

Low-Temperature Two-Phase Microchannel Cooling for High-Heat-Flux Thermal Management of Defense Electronics

Jaeseon Lee and Issam Mudawar

Abstract—For a given heat sink thermal resistance and ambient temperature, the temperature of an electronic device rises fairly linearly with increasing device heat flux. This relationship is especially problematic for defense electronics, where heat dissipation is projected to exceed 1000 W/cm^2 in the near future. Direct and indirect low-temperature refrigeration cooling facilitate appreciable reduction in the temperature of both coolant and device. This paper explores the benefits of cooling the device using direct and indirect refrigeration cooling systems. In the direct cooling system, a microchannel heat sink serves as an evaporator in a conventional vapor compression cycle using R134a as working fluid. In the indirect cooling system, HFE 7100 is used to cool the heat sink in a primary pumped liquid loop that rejects heat to a secondary refrigeration loop. Two drastically different flow behaviors are observed in these systems. Because of compressor performance constraints, mostly high void fraction two-phase patterns are encountered in the R134a system, dominated by saturated boiling. On the other hand, the indirect refrigeration cooling system facilitates highly subcooled boiling inside the heat sink. Both systems are shown to provide important cooling benefits, but the indirect cooling system is far more effective at dissipating high heat fluxes. Tests with this system yielded cooling heat fluxes as high as 840 W/cm^2 without incurring critical heat flux (CHF). Results from both systems are combined to construct an overall map of performance trends relative to mass velocity, subcooling, pressure, and surface tension. Extreme conditions of near-saturated flow, low mass velocity, and low pressure produce “micro” behavior, where macrochannel flow pattern maps simply fail to apply, instabilities are prominent, and CHF is quite low. On the other hand, systems with high mass velocity, high subcooling, and high pressure are far more stable and yield very high CHF values; two-phase flow in these systems follows the fluid flow and heat transfer behavior as well as the flow pattern maps of macrochannels.

Index Terms—Electronics cooling, high heat flux, microchannel flow, phase change.

NOMENCLATURE

AR Aspect ratio of microchannel.
 Bo Boiling number.
 c_p Specific heat.

D_h Hydraulic diameter.
 G Mass velocity.
 h Heat transfer coefficient.
 H_{ch} Microchannel height.
 h_{fg} Latent heat of vaporization.
 H_{tc} Distance between thermocouple and base of microchannel.
 Ja^* Modified Jacob number.
 k Thermal conductivity.
 L Length of microchannel.
 m Fin parameter.
 N Total number of microchannels in heat sink.
 Nu Nusselt number.
 P Pressure.
 ΔP Pressure drop across micro-channel.
 Pr Prandtl number.
 q'' Heat flux through heat sink base area.
 q_p'' Mean heat flux through three conducting walls of microchannel.
 Re Reynolds number.
 R_{th}'' Thermal resistance.
 T Temperature.
 T_f Local bulk liquid temperature.
 T_{tc} Measured copper temperature.
 $T_{w,b}$ Local base-wall temperature of microchannel.
 W_{ch} Microchannel width.
 We Weber number.
 We^* Modified Weber number.
 W_w Half-width of wall separating microchannels.
 X Martinelli parameter.
 x_e Thermodynamic equilibrium quality.
 z Stream-wise coordinate.

Greek Symbols:

β, β^* Channel aspect ratio ($\beta^* < 1$).
 η Fin efficiency.
 μ Viscosity.
 ρ Density.

Manuscript received April 03, 2008; revised July 15, 2008. First published February 06, 2009; current version published July 22, 2009. This work was supported by the Office of Naval Research (ONR). This work was recommended for publication by Associate Editor R. Prasher upon evaluation of the reviewers comments.

J. Lee is with the United Technologies Research Center (UTRC), E. Hartford, CT 06108 USA.

I. Mudawar is with the Boiling and Two-Phase Flow Laboratory (BTPFL) and the Purdue University International Electronic Cooling Alliance (PIECA), West Lafayette, IN 47907-2088 USA (e-mail: mudawar@ecn.purdue.edu).

Digital Object Identifier 10.1109/TCAPT.2008.2005783

- σ Surface tension.
 ϕ Fluid phase.

Subscripts:

- 3 Based on three-sided heating of rectangular microchannel.
c Half-way along microchannel.
ch Microchannel.
e Thermodynamic equilibrium
f Liquid.
fo Liquid only.
g Vapor.
in Microchannel inlet.
out Microchannel outlet.
s Solid.
sat Saturation.
sp Single-phase.
tc Thermocouple.
tp Two-phase.
w Channel base wall.

I. INTRODUCTION

A. Application of Refrigeration Cooling

THE PAST 30 years have witnessed unprecedented enhancement in chip performance, brought about mostly by advances in microminiaturization of electronic circuits. As the number of circuits integrated in a single device increased, so did the amount of dissipated heat. This problem is further compounded when multiple devices are packaged in close proximity to one another on a single circuit board, especially in systems containing a multitude of circuit boards.

During the 1980s, device heat dissipation was easily managed using air-cooled heat sinks, and any increases in device heat flux could be tackled with larger and more effective heat sink designs. It was not until the early 1990s, as device heat flux approached 100 W/cm^2 , that the electronics industry was forced to begin exploring liquid cooling solutions. Recent liquid cooling research efforts have culminated in numerous cooling solutions that are capable of tackling mostly the $50\text{--}150 \text{ W/cm}^2$ range [1].

Defense electronics represent a specialized class of devices that have for the most part followed the heat dissipation trends of commercial devices. However, a new generation of devices for defense radars and directed-energy laser and microwave weapons are approaching 1000 W/cm^2 [1], which exceeds the capabilities of today's most advanced liquid cooling solutions. This trend is the primary motivation for the present study. The goal here is to develop advanced thermal management schemes that can remove very large heat fluxes from advanced defense electronics while maintaining device temperatures below 125°C .

The difficulty in implementing even the most aggressive liquid cooling scheme is that, for a given resistance between

the device and coolant and fixed coolant temperature, the device temperature increases fairly linearly with increasing heat dissipation rate. This relationship could easily bring the temperature of the device above its maximum limit when dissipating high heat fluxes. For a device operating slightly below its maximum temperature limit, dissipating increasing amounts of heat requires reducing the temperature of the liquid coolant. This trend would ultimately drop the coolant temperature below ambient temperature, requiring the use of a refrigeration system to sustain the cooling. Further reducing the coolant temperature allows the device to operate well below its maximum temperature limit. Various refrigeration cooling schemes have been suggested to achieve this objective [2], [3]. Of those, vapor compression systems have attracted the most attention because of their relatively high cooling capacity at temperature of interest [4]–[7].

Refrigeration cooling can be implemented in two different configurations. In the first *direct-refrigeration-cooling* configuration, the cooling module is incorporated as an evaporator in a vapor compression cycle, and the refrigerant serves as coolant for the electronic device. The alternative *indirect-refrigeration-cooling* configuration involves using two fluid loops. Heat from the device is rejected to a primary coolant circulating through a pumped liquid loop that rejects the heat via a heat exchanger to refrigerant flowing in a separate vapor compression cycle.

In recent years, microchannel cooling has attracted the most attention of any cooling scheme for high-flux electronic cooling. The small hydraulic diameter of a microchannel heat sink greatly increases the convective heat transfer coefficient, especially where the coolant is allowed to vaporize along the channel. Microchannel heat sinks also possess attributes that are of special importance to electronics cooling such as compactness and minimal coolant usage. Allowing the coolant to vaporize along the microchannel contributes the additional benefits of significant enhancement in the heat transfer coefficient and better axial fluid and surface temperature uniformity, dictated mostly by the coolant's saturation temperature, compared to single-phase microchannel flow. However, two-phase microchannel heat sinks are not without shortcomings. Small hydraulic diameter can lead to appreciable pressure drop and therefore high pumping power consumption. Two-phase microchannel heat sinks are also prone to different types of flow, pressure, and temperature oscillations [8]. The cooling performance of a heat sink depends on whether it is used in a direct- or indirect-refrigeration-cooling configuration. As discussed below, these configurations yield two drastically different types of flow boiling, *saturated* and *subcooled*.

B. Direct Refrigeration Cooling and Saturated Microchannel Flow Boiling

Using a microchannel heat sink as an evaporator in a direct-refrigeration cooling system requires that the coolant's operating conditions conform to those of a vapor compression cycle. First, a refrigerant (R134a for most modern systems) is used as the primary coolant. The refrigerant enters the microchannel evaporator as a two-phase mixture and exits as saturated or superheated vapor as required by most refrigeration compressors. Under these conditions, as well as in most

published microchannel studies, the coolant undergoes rapid change of phase into a high void fraction mixture. Therefore, slug and annular flow are often cited as dominant flow regimes for this cooling configuration. Hence, two-phase pressure drop and heat transfer coefficient models are based mostly on these regimes [9]–[21].

The authors of the present study examined the performance of a microchannel heat sink that served as an evaporator in a direct refrigeration cooling cycle using R134a as working fluid [20], [21]. Aside from developing new correlations for two-phase pressure drop and heat transfer coefficient, they provided practical insight into the implementation of the direct-refrigeration-cooling configuration. They showed that the throttling valve offers significant stiffening to the refrigeration cycle, suppressing the large pressure oscillations common to microchannel heat sinks.

C. Indirect Refrigeration Cooling and Subcooled Microchannel Flow Boiling

Using a separate loop for the primary coolant provides greater flexibility in attaining the desired microchannel heat sink's inlet conditions. Most importantly, the coolant does not have to be maintained in a near-saturated or superheated state as required by the compressor in the direct-refrigeration-cooling configuration.

Subcooled boiling occurs when the coolant is supplied to the heat sink below saturation temperature, corresponding to a thermodynamic equilibrium quality below zero. The quality rises along the microchannel and, if the channel is long enough, the flow may ultimately transition to saturated boiling. However, the short length of a microchannel heat sink precludes such transition, especially for high mass velocities and highly subcooled inlet conditions. Because of large differences in void fraction, the heat transfer mechanism for subcooled boiling is categorically different from that for saturated boiling. In subcooled boiling, liquid flow is more abundant and phase-change occurs mostly by bubble formation at the wall. In general, much higher critical heat flux (CHF) values are possible with subcooled flow boiling than with saturated. Furthermore, CHF mechanism for subcooled boiling is fundamentally different from that for saturated boiling. Subcooled boiling CHF (also referred to as “departure from nucleate boiling”) is the result of localized vapor blanket formation along the heated wall, and occurs despite the abundance of liquid in the core. On the other hand, CHF in saturated boiling occurs in the channel's downstream liquid deficient region as a result of dry-out of the annular liquid film.

Research on subcooled flow boiling in microchannels predates microchannel electronic cooling studies. This form of cooling was the subject of intense study since the mid 1970s at the Massachusetts Institute of Technology Energy Laboratory for cooling of electrodes in magnetohydrodynamic energy converters and turbine blades [22]. A number of subsequent studies demonstrated the enormous cooling potential of subcooled flow boiling. Mudawar and Bowers [23] showed highly subcooled and high mass velocity flow boiling of water in small diameter tubes could safely dissipate up to 27 000 W/cm².

Unfortunately, the dielectric coolants recommended for electronics cooling possesses poor thermal transport properties. This

renders the task of achieving very high heat fluxes while maintaining the device temperature below 125 °C quite elusive.

This paper explores the cooling potential of two-phase microchannel heat sinks when combined with refrigeration cooling. Both direct and indirect refrigeration cooling are considered, and dominant two-phase flow patterns explored. The pressure-drop and heat transfer performances are discussed for each configuration. These and other practical considerations are used to identify the merits and drawbacks of each configuration, especially the ability to meet the high-flux cooling requirements of defense electronics.

II. EXPERIMENTAL METHODS

A. Direct Refrigeration Cooling System

Fig. 1(a) shows a schematic diagram of the test loop used to simulate a direct-refrigeration-cooling system. The microchannel test module is incorporated as evaporator in a fairly conventional vapor compression cycle using R134a as working fluid. The loop utilizes a rotary compressor powered by a dc source and a finned-tube air-cooled condenser. The condenser's air flow is regulated by a variac to control the condenser's exit subcooling. A glass flow meter is used to confirm liquid state at the condenser outlet as well as measure volumetric flow rate. A manual metering valve situated upstream of the microchannel evaporator throttles the flow between the high condenser pressure and low evaporator pressure.

Fig. 1(b) shows the construction of the test module used in the direct-refrigeration-cooling system. Fifty-three 231- μm -wide and 713- μm -tall microchannels are cut into the top 2.53-cm-long surface of an oxygen-free copper block. This block is inserted into an insulating fiberglass plastic housing and covered atop with a transparent plate of polycarbonate plastic. Heat is provided by three cartridge heaters inserted into the lower enlarged portion of the copper block. Coolant temperature and pressure are measured in the housing plenums both upstream and downstream of the microchannels. The copper block temperature is measured by a T-type thermocouple inserted beneath the microchannels. Table II provides details of the microchannel geometry.

Operating conditions for the microchannel in the direct-refrigeration-cooling system are as follows: inlet pressure of $P_{\text{in}} = 1.44 - 6.60$ bar, inlet quality of $x_{e,\text{in}} = 0.001 - 0.25$, outlet quality of $x_{e,\text{out}} = 0.49$ —superheat, and mass velocity of $G = 127 - 654$ kg/m²s. Further details of this system are available elsewhere [20], [21].

B. Indirect Refrigeration Cooling System

Fig. 2(a) shows the flow diagram of the indirect-refrigeration-cooling system. Here, the vapor compression system is completely isolated from the primary cooling loop containing the microchannel module. The working fluid in the primary cooling loop is 3M's Novec fluid HFE 7100. This fluid has a low freezing point below -100 °C and a moderate boiling point of 60 °C at atmospheric pressure. Table I compares representative values of the thermophysical properties of HFE 7100 to those of R134a.

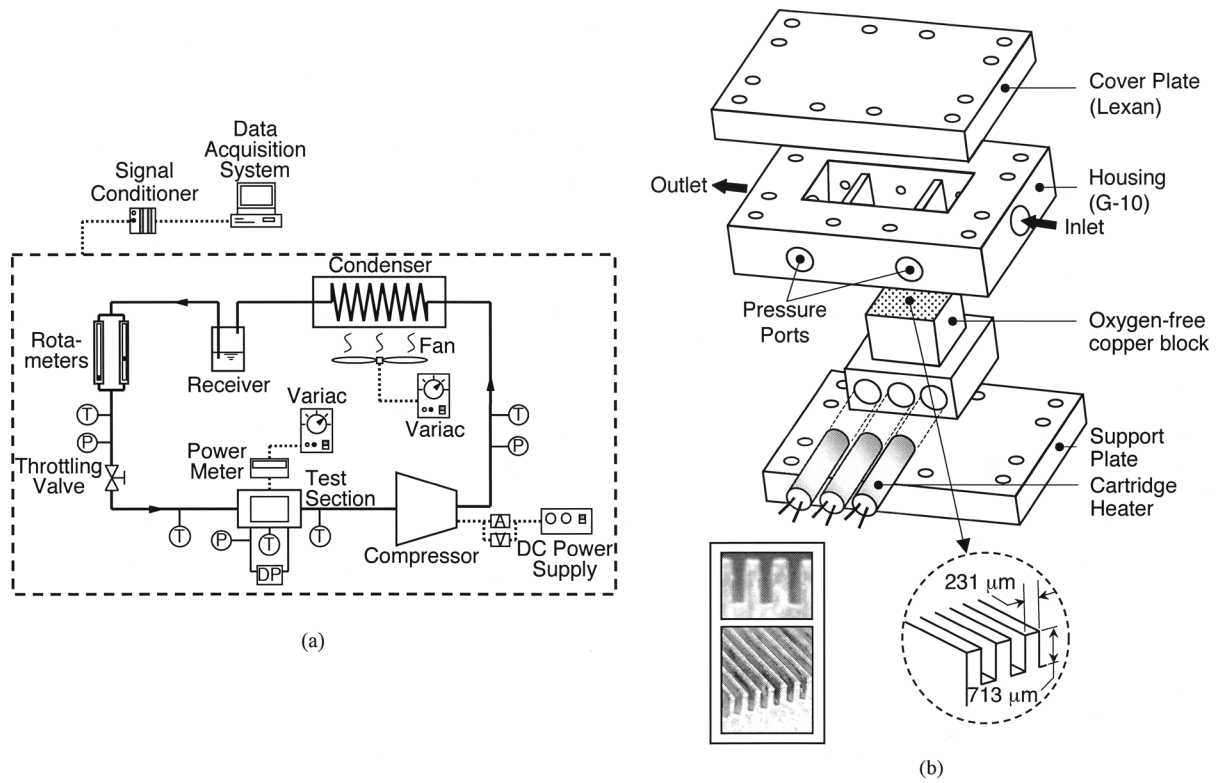


Fig. 1. (a) Schematic diagram of flow loop and (b) construction of test module for direct refrigeration cooling system.

TABLE I
SUMMARY OF SATURATED THERMOPHYSICAL PROPERTIES OF R134a AND HFE 7100 AT 1.0 BAR

| | T_{sat} (°C) | h_{fg} (kJ/kg) | ρ_f (kg/m ³) | ρ_g (kg/m ³) | σ (mN/m) | μ_f (kg/m.s) |
|----------|-------------------|---------------------|----------------------------------|----------------------------------|--------------------|-----------------------|
| R134a | -26.37 | 217.2 | 1377.8 | 5.19 | 15.5 | 3.79×10^{-4} |
| HFE 7100 | 59.63 | 111.7 | 1372.7 | 9.58 | 15.7 | 8.26×10^{-4} |

TABLE II
MICROCHANNEL TEST MODULE DIMENSIONS

| | W_{ch} (μm) | W_w (μm) | H_{ch} (μm) | H_c (mm) | AR | D_h (μm) | L (cm) | N |
|-----------------------------|------------------|---------------|------------------|---------------|------|---------------|-------------|-----|
| Direct Cooling (R134a) | 231 | 114 | 713 | 7.67 | 3.09 | 349 | 2.53 | 53 |
| Indirect Cooling (HFE 7100) | 235 | 115 | 577 | 4.50 | 2.46 | 334 | 1.0 | 11 |

As shown in Fig. 2(a), HFE 7100 liquid is pumped through a heat exchanger to reduce its temperature by rejecting heat to the secondary refrigeration loop. Exiting the heat exchanger, the HFE 7100 liquid passes through a filter followed by a Coriolis mass flow meter before entering the microchannel test module. Throttling valves situated upstream and downstream of the test module are used to regulate both flow rate and the test module's outlet pressure.

Fig. 2(b) illustrates the construction of the microchannel test module. This module is fairly similar to the one used in the direct-refrigeration-cooling system, save base area and number of cartridge heaters. Table II provides the detailed geometry of

the indirect cooling microchannel test module. Further details of this test module are available elsewhere [24], [25].

The indirect-refrigeration-cooling experiments were performed at two test module inlet temperatures, -30°C and 0°C , at a constant outlet pressure of 1.138 bar. Mass velocity covered a range of $G = 1330 - 13,400 \text{ kg/m}^2\text{s}$.

III. PRESSURE DROP RESULTS

As indicated earlier, high pressure drop is a primary concern in the implementation of microchannel cooling. One reason for the high pressure drop is the small hydraulic diameter that is required to achieve high convective heat transfer coefficients. Another reason is vapor production along the microchannels, which increases both the frictional and accelerational pressure gradients along the microchannel as well as overall pressure drop. A third reason is that high heat fluxes require high mass velocities, which also contribute high pressure drop. However, the role and significance of each of these parameters differs greatly between saturated and subcooled flows.

When comparing saturated and subcooled flows, it is useful to examine pressure drop per unit microchannel length, especially

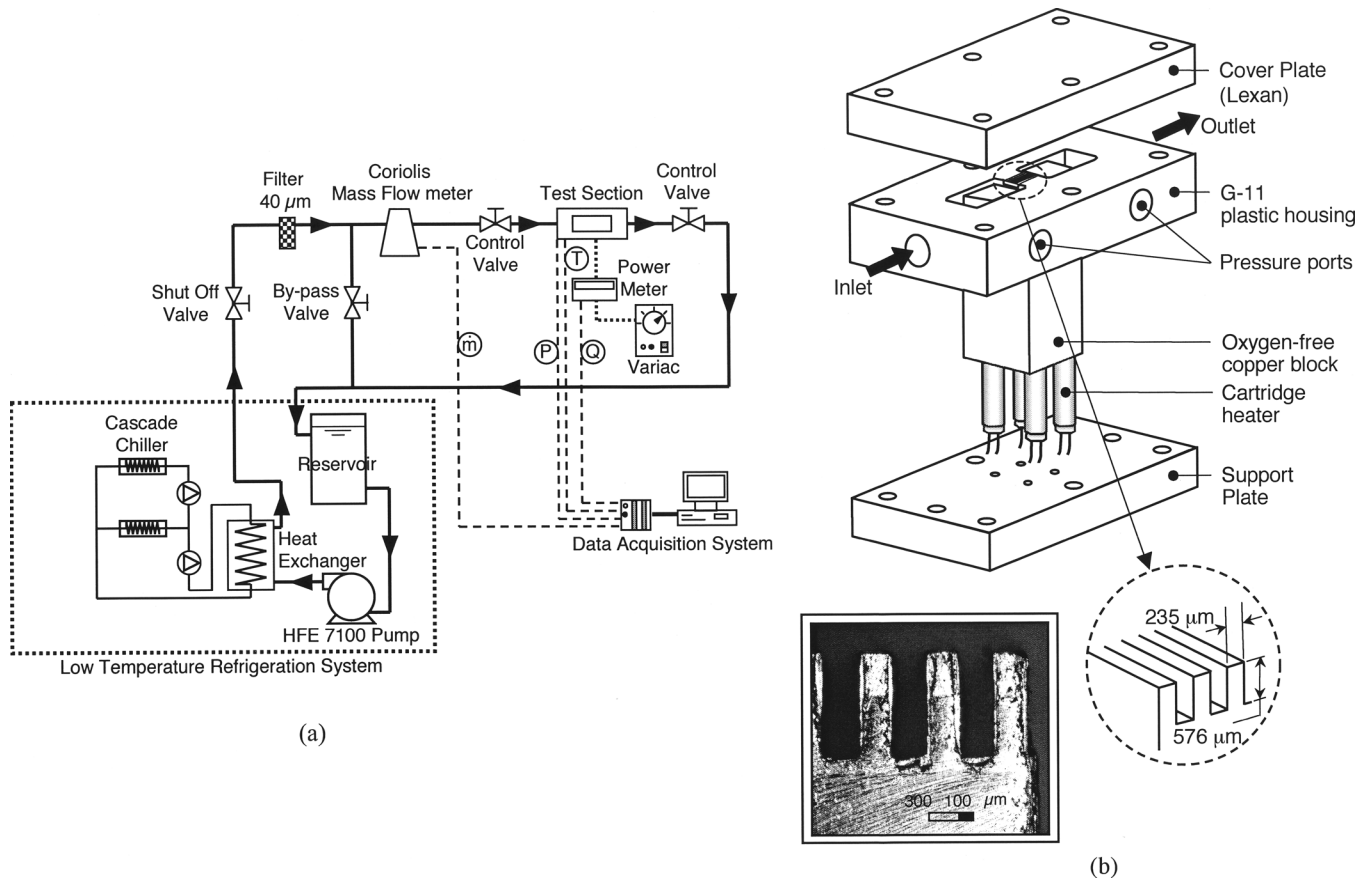


Fig. 2. (a) Schematic diagram of flow loop and (b) construction of test module for indirect refrigeration cooling system.

for different microchannel lengths. Such experimental data are presented in Fig. 3. To calculate the microchannel pressure drop, the inlet plenum pressure loss and outlet plenum pressure recovery are subtracted from the total pressure drop measured by pressure transducers connected to the plenums. Details of the relations used to account for these effects are available elsewhere [8], [20].

More than attempting to directly compare results for R134a direct refrigeration cooling and HFE 7100 indirect cooling, Fig. 3 is intended to identify trends in the variation of pressure drop per unit length as well as gain a better understanding of the underlying physical mechanisms. It should also be emphasized that significantly higher mass velocities are possible with the indirect-refrigeration-cooling system, given the greater flexibility in increasing coolant flow rate with this system compared to the direct-refrigeration-cooling system. The higher pressure drop values in Fig. 3(b) can be explained by the pressure drop being proportional to the square of mass velocity. Notice that any differences in pressure drop due to microchannel geometry are minimized by comparing data for similarly sized microchannels.

Aside from the pressure drop trends, a noteworthy comparison of Fig. 3(a) and (b) is the magnitude of pressure drop per unit length for the lowest mass velocity case for HFE 7100 versus the highest mass velocity case for R134a for the same heat flux range of $q'' = 0 - 100 \text{ W/cm}^2$. Despite a nearly 2.8 times greater mass velocity for the former, pressure drop is much smaller than for R134a. Aside from the obvious differences in

thermophysical properties, the high-pressure drop of saturated boiling R134a is the result of high void fraction. In contrast, the subcooled boiling HFE 7100 system maintains single-phase liquid flow and/or minimal void fraction over the noted heat flux range.

The second noteworthy difference between Fig. 3(a) and (b) is overall shape of the pressure drop characteristics. A key factor that influences this shape is the onset of boiling at a particular heat flux value. Thereafter, pressure drop begins to increase appreciably due the strong influence of void fraction on pressure drop. Mass velocity can complicate the pressure drop trends for certain conditions.

The R134a data in Fig. 3(a) correspond exclusively to saturated boiling conditions at the microchannel inlet brought about by flashing across the throttling valve. Saturated or superheated conditions are maintained along the length of the microchannel. For each mass velocity, Fig. 3(a) shows pressure drop rises more rapidly at low heat fluxes than at high fluxes. This trend may be explained by downstream microchannel dry-out at high fluxes versus predominantly slug and annular flow along the entire microchannel at low fluxes. The extent of the downstream dry-out region increases with increasing heat flux, reducing the fraction of the length undergoing high pressure saturated boiling. Fig. 3(a) shows a predictable monotonic trend of increasing pressure drop with increasing mass velocity.

The HFE 7100 pressure drop data in Fig. 3(b) show far more complicated roles for heat flux and mass velocity. Notice how pressure drop for each mass velocity first decreases slightly with

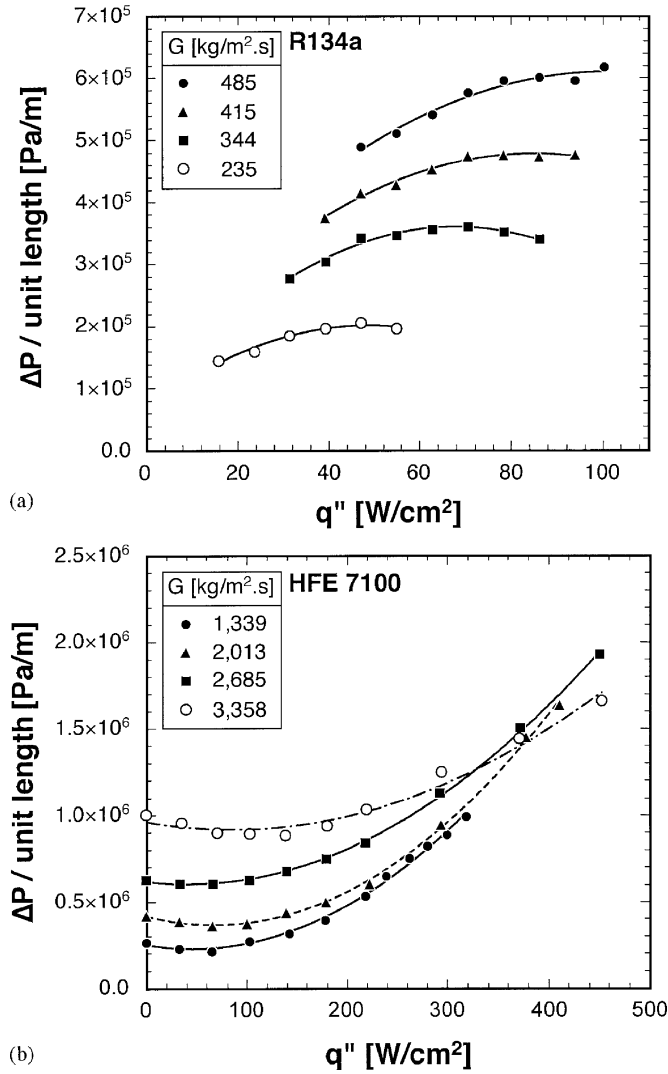


Fig. 3. Variation of pressure drop per unit microchannel length with heat flux for (a) direct refrigeration cooling system and (b) indirect refrigeration cooling system.

increasing heat flux. This low heat flux region corresponds to single-phase liquid flow, and the decreasing pressure drop is the result of a reduction of liquid viscosity with increasing temperature. This trend is reversed once nucleate boiling commences inside the microchannel, resulting in a minimum in the pressure drop dependence on heat flux. It should be emphasized that all data in Fig. 3(b) correspond to subcooled boiling conditions, where bubbles are generated in a thin superheated liquid layer at the wall while the bulk liquid core is subcooled. As bubbles detach from the wall, they have a tendency to condense in the liquid core, which explains the relatively low void fractions encountered in subcooled boiling. The milder increase in pressure drop with increasing heat flux at $G = 3358 \text{ kg/m}^2 \cdot \text{s}$ compared to the lower mass velocities is the result of stronger condensation effects at higher mass velocities.

Fig. 4 shows representative images for saturated R134a and subcooled HFE 7100 flows that confirm the aforementioned influence of void fraction in the pressure drop trends. Saturated boiling spans most two-phase flow regimes, bubbly, slug, elongated slug, annular, and dry out, though bubbly flow is only observed at very low heat fluxes. Fig. 4(a) captures conditions

along the middle section of the microchannel corresponding to the most frequently observed high void patterns of elongated slug flow and annular flow for R134a. On the other hand, Fig. 4(b) depicts the bubbly flow pattern that dominated the HFE 7100 subcooled boiling tests.

Additional extensive flow visualization results are available in previous studies by the present authors for both saturated boiling [20] and subcooled boiling [25]. These studies provide comprehensive assessments of prior pressure drop correlations and recommend new correlations with greater accuracy in predicting experimental data.

IV. HEAT TRANSFER RESULTS

A. Reduction of Heat Transfer Coefficient Data

Fig. 5 shows a unit cell consisting of a single microchannel, surrounding copper half-walls, and portion of the top cover plate. A simplified fin model of the copper walls is used to construct an energy balance for this unit cell. Equating the heat influx to the unit cell through the bottom solid wall to the heat efflux by flow boiling along the microchannel bottom wall and sidewalls yields

$$q'' (W_{ch} + 2W_w) = h(T_{w,b} - T_f)(W_{ch} + 2\eta H_{ch}) \quad (1)$$

where η is the fin efficiency. Since the top wall is adiabatic, the fin efficiency is given by [26]

$$\eta = \frac{\tanh(m H_{ch})}{m H_{ch}} \quad (2)$$

where m is the fin parameter defined as

$$m = \sqrt{\frac{h}{k_s W_w}} \quad (3)$$

The fin base temperature $T_{w,b}$ is calculated using the assumption of one-dimensional heat diffusion between the plane of the thermocouple embedded in the copper block and the plane containing the channel base

$$T_{w,b} = T_{tc} - \frac{q'' H_{tc}}{k_s} \quad (4)$$

The fluid temperature T_f , in (1) is the fluid bulk temperature halfway along the microchannel. This temperature is determined differently for the R134a and HFE 7100 systems. For the R134a saturated boiling tests T_f is based on pressure at the same location determined from the measured inlet pressure and pressure drop correlation scheme presented in [21]. For the HFE 7100 subcooled boiling tests, T_f is assumed equal to the average of the measured inlet and outlet temperatures of the subcooled flow.

Equations (1) and (2) are used to determine h since all other parameters are easily measured or calculated.

B. Heat Transfer Coefficient Results

Differences in system operation caused the R134a and HFE 7100 tests to be performed in different ways. Since the compressor in the direct refrigeration cooling system is sensitive to changes in heat load, varying power input to the test module (to

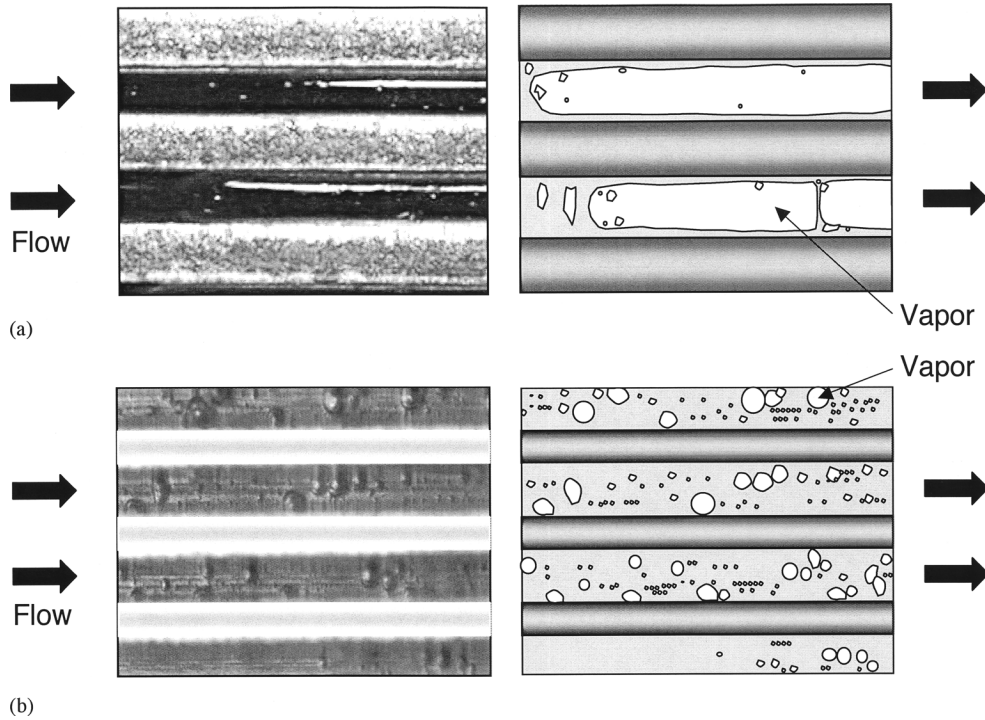


Fig. 4. Microchannel flow boiling pattern in central region of microchannels for (a) R134a saturated boiling (direct refrigeration cooling system) at $G = 163 \text{ kg/m}^2 \cdot \text{s}$, $x_{e,c} = 0.53$, and $q'' = 31.6 \text{ W/cm}^2$, and (b) HFE 7100 subcooled boiling (indirect refrigeration cooling system) at $G = 1,339 \text{ kg/m}^2 \cdot \text{s}$, $x_{e,c} = -0.57$, and $q'' = 102.3 \text{ W/cm}^2$.

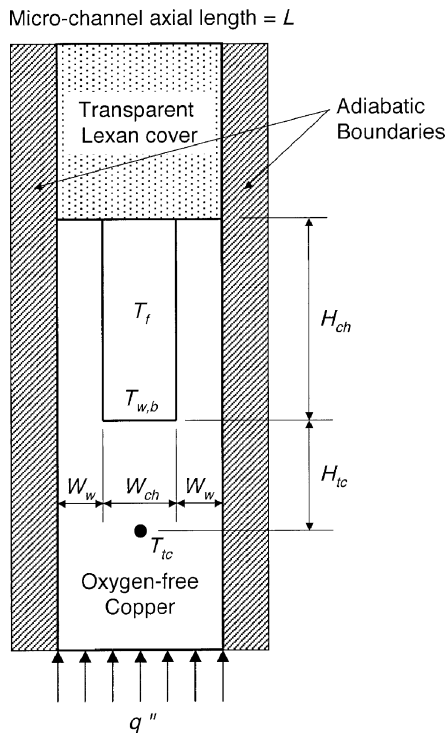


Fig. 5. Unit cell used to infer heat transfer coefficient in microchannel.

alter heat flux) causes changes in flow rate as well as all key flow parameters of the test module. Therefore, the R134a tests were performed by fixing the heat input and varying the flow rate with the aid of the throttling valve. The HFE 7100 system provided far greater flexibility in controlling parameters as well

as decoupling flow rate from heat input. These experiments were performed by increasing heat flux while fixing flow rate.

Fig. 6 shows local heat transfer coefficient data from each test section halfway along the microchannel plotted against thermodynamic equilibrium quality, which is defined as

$$x_e = \frac{h_f - h_{f,sat}}{h_{fg}} \quad (5)$$

Notice that x_e values in Fig. 6 are positive for all the R134a saturated boiling data and negative for the HFE 7100 subcooled boiling data.

Fig. 6(a) shows R134a saturated boiling produces very high heat transfer coefficient values for the low x_e range corresponding to mostly bubbly flow. However, these values drop sharply with increasing quality in the annular regime and ultimately converge into heat transfer coefficient values for pure vapor flow. As discussed in [21], the high heat transfer coefficients at low quality are unique to low surface tension fluids but far less prevalent for high surface tension fluids. Low surface tension fluids produce relatively small bubbles, allowing the bubbly and slug flow regimes to persist for certain operating condition. However, nucleating bubbles in high surface tension fluids such as water are much larger, tending to quickly fill the channel and cause abrupt transition into annular flow. This phenomenon allows R134a to yield heat transfer coefficient values comparable to those of water, despite the much poorer thermophysical properties of R134a. However, this attribute of R134a is compromised by the system requirements of the vapor compression cycle. On one hand, Fig. 6(a) proves quality must be kept low to achieve high h values. On the other hand,

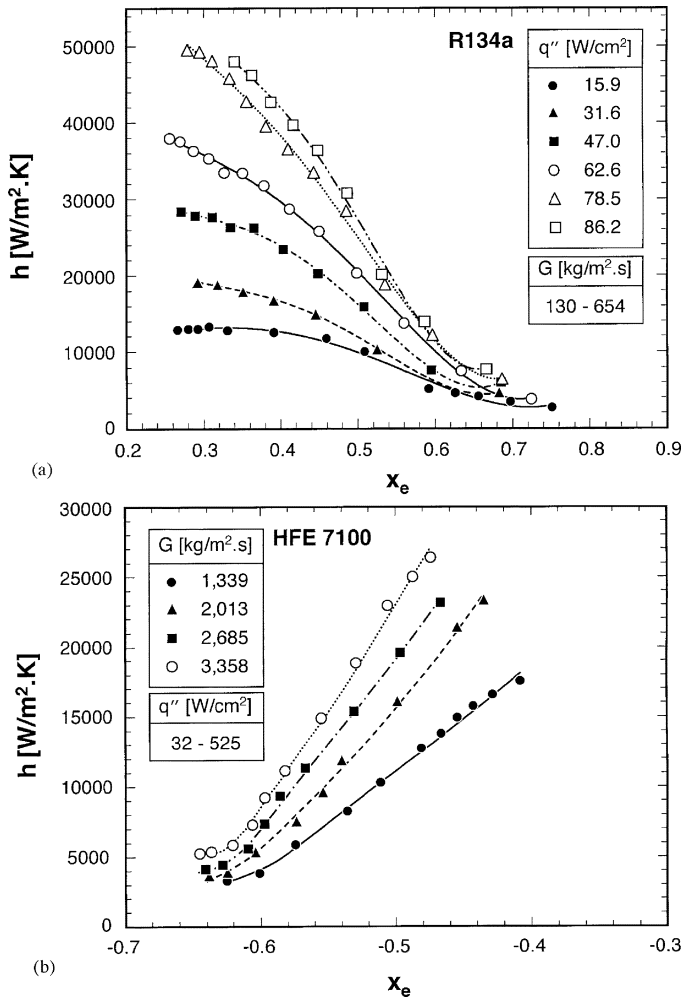


Fig. 6. Variation of measured local heat transfer coefficient with equilibrium quality for different heat fluxes and mass velocities for (a) R134a saturated boiling in direct refrigeration cooling system and (b) HFE 7100 subcooled boiling in indirect refrigeration cooling system.

the compressor favors saturated or superheated vapor conditions. This requires the use of a secondary heater or phase separator downstream of the test module, which compromises the coefficient of performance of the vapor compression cycle. Another drawback of the R134a direct refrigeration system is the relatively large wall temperature rise along the flow direction, which is caused by rapid succession of different flow patterns along the microchannel [27].

Fig. 6(b) shows the heat transfer coefficient for HFE 7100 is constant for very low x_e values corresponding to pure liquid flow. The heat transfer coefficient begins to increase once nucleation commences as subcooled boiling is initiated along the microchannel.

C. Boiling Curve and Critical Heat Flux Trends

Fig. 7 shows boiling curves for R134a and HFE 7100. The absence of single-phase liquid data for R134a in Fig. 7(a) is the result of the aforementioned compressor requirement. Another feature of the R134a data is the difficulty identifying CHF. One reason for this difficulty is the relatively small heat flux range of the direct refrigeration cooling tests. Another reason is the

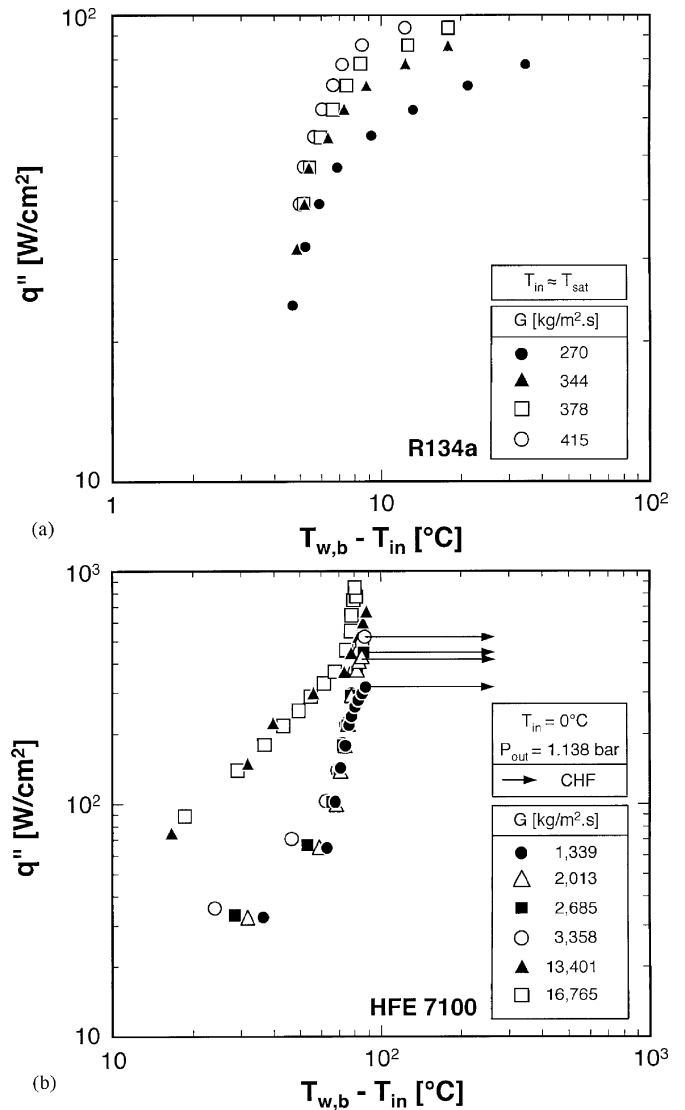


Fig. 7. Boiling curves for (a) R134a saturated boiling in direct refrigeration cooling system and (b) HFE 7100 subcooled boiling in indirect refrigeration cooling system.

ability of the copper block to sustain downstream dry-out by axial conduction.

Fig. 7(b) shows boiling curves for HFE 7100. The ability of the indirect refrigeration cooling system to achieve high mass velocities allowed these tests to dissipate very high fluxes. Notice the highest mass velocity condition facilitating the dissipation of over 840 W/cm², even though this particular test was terminated before CHF in order to prevent excessive overheating of the test module components. Overall, increasing mass velocity increased both the single-phase heat transfer coefficient and CHF; however, data appear to converge in the nucleate boiling region.

D. Thermal Resistance Trends

As indicated earlier, it is difficult to compare the performances of the direct and indirect refrigeration systems based on heat transfer coefficient values. However, somewhat similar solid wall temperatures were maintained in both systems for a

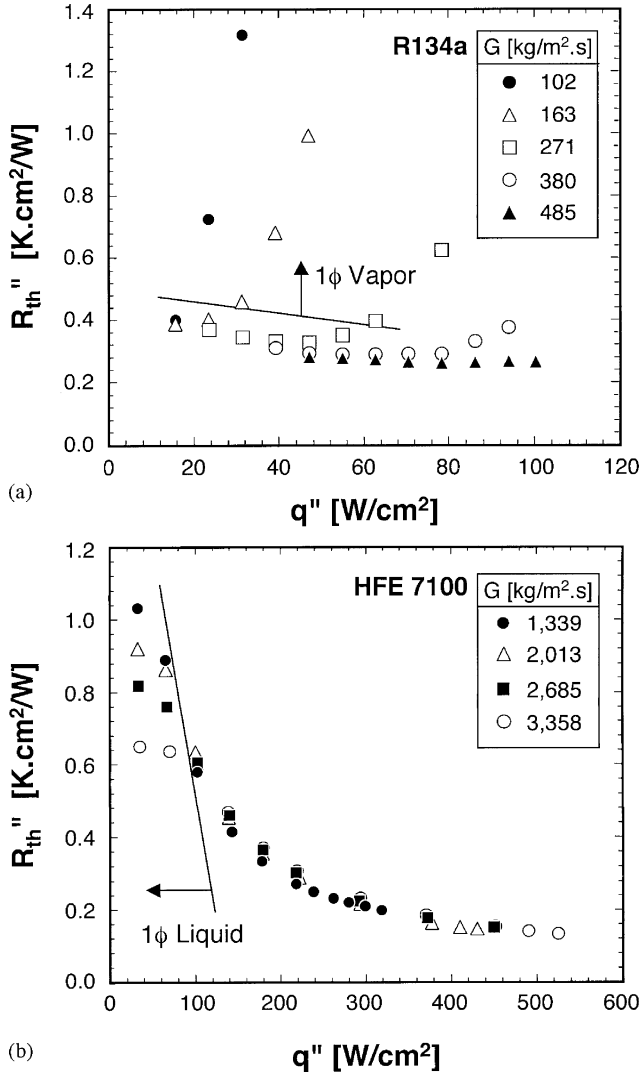


Fig. 8. Convective thermal resistance versus heat flux for (a) R134a saturated boiling in direct refrigeration cooling system and (b) HFE 7100 subcooled boiling in indirect refrigeration cooling system.

given value of superheat. This provided a basis for comparing the thermal performances of the two systems based on thermal resistance. The convective thermal resistance is defined from a chip cooling perspective (rather than simply the reciprocal of h) as

$$R_{th}'' = \frac{T_{w,b} - T_f}{q''} \quad (6)$$

Fig. 8 compares the resistance characteristics of the two systems. The R134a system is capable of resistances as low as $0.25 \text{ K} \cdot \text{cm}^2/\text{W}$; however, these resistance values are maintainable up to only $100 \text{ W}/\text{cm}^2$ because of the dry-out effects. On the other hand, the indirect cooling system facilitates much broader ranges of both mass flux and CHF, and thermal resistance values drop sharply once subcooled boiling commences along the microchannels. The resistance for HFE 7100 decreases monotonically with increasing heat flux, culminating in values around $0.10 \text{ K} \cdot \text{cm}^2/\text{W}$.

TABLE III
HEAT TRANSFER COEFFICIENT CORRELATIONS

| Correlations | |
|------------------------|----------------------------------------------------------------------------------------------------------------------------------------------------------------|
| Saturated Boiling [17] | For $0.05 < x_e \leq 0.55$ $h_{sp} = 436.48 Bo^{0.522} We_{fo}^{0.351} X^{0.665} h_{sp,f}$ |
| | For $0.55 < x_e$ $h_{sp} = \max\left[108.6 X^{1.665} h_{sp,g}, h_{sp,g}\right]$ |
| Subcooled Boiling [21] | $Bo = \frac{q''}{G h_{fg}}, We_{fo} = \frac{G^2 D_h}{\rho_f \sigma}, X^2 = \frac{(dp/dz)_f}{(dp/dz)_g}, h_{sp,f} = \frac{Nu_3 k_f}{D_h}$ |
| | $h_{sp,g} = \frac{Nu_3 k_g}{D_h} \text{ for laminar gas flow}$ |
| | $Nu_3 = 8.235(1 - 1.883\beta^* + 3.767\beta^{*2} - 5.814\beta^{*3} + 5.361\beta^{*4} - 2.0\beta^{*5})$ |
| | $\beta^* = \frac{H_{ch}}{W_{ch}} \text{ or } \frac{H_{ch}}{W_{ch}}, (\beta^* < 1)$ $Nu_{sp,g} = 0.023 Re_g^{0.8} Pr_g^{0.4} \text{ for turbulent gas flow}$ |
| | $\frac{Nu_{sp}}{Nu_p} = 90.0 Bo^{0.9} Ja^{*-0.98} We^{*0.15} \beta^{*0.42}$ |
| | $Ja^* = \frac{c_{p,f} \Delta T_{sub,m}}{h_{fg}}, We^* = \frac{G^2 D_h}{(\rho_f - \rho_g) \sigma}, \text{ and } \beta = \frac{H_{ch}}{W_{ch}}$ |

E. Overall Assessment of Direct Refrigeration and Indirect Refrigeration Systems

To provide a more quantitative comparison of the direct refrigeration and indirect refrigeration systems, previous correlations developed by the authors are used. Table III summarizes microchannel heat transfer correlations for saturated boiling [21] and subcooled boiling [25]. For a more systematic comparison, the same geometry is used and same mean heat flux, $q_p'' = 200 \text{ W}/\text{cm}^2$, is assumed for the three metal surfaces of the microchannel. For the R134a saturated boiling case, quality varies from 0.1 at the microchannel inlet to 1.0 at the outlet. The HFE 7100 case involves subcooled boiling with an inlet quality of -1.0 and an outlet quality -0.1 . The mass velocity required to achieve these conditions is determined from the following equations.

$$\begin{aligned} \text{Saturated boiling: } q_p'' &= (W_{ch} + 2W_w) L \\ &= G (W_{ch} H_{ch}) (x_{e,out} - x_{e,in}) h_{fg} \quad (7) \\ \text{Subcooled boiling: } q_p'' &= (W_{ch} + 2W_w) L \\ &= G (W_{ch} H_{ch}) c_{p,f} (T_{out} - T_{in}). \quad (8) \end{aligned}$$

Table IV lists all conditions used in this comparative analysis.

Fig. 9 shows the results of the comparative study. Shown are variations of the two-phase heat transfer coefficient and the surface-to-fluid temperature difference along the microchannel; the surface temperature used here is the base wall temperature of the microchannel. Fig. 9(a) show the results for R134a saturated boiling. Discontinuities in the two curves in this figure are the result of using different correlations corresponding to low quality versus high quality. As discussed earlier, the heat transfer coefficient is very high near the inlet, but decreases sharply towards the outlet. Correspondingly, the wall temperature is lowest near the inlet but increases appreciably at the outlet. Fluid temperature changes very slightly along the microchannel since it is equal to the saturation temperature.

TABLE IV
CONDITIONS USED IN COMPARATIVE STUDY ($P_{out} = 1 \text{ bar}$, $q'' = 200 \text{ W/cm}^2$)

| | W_{ch} (μm) | W_w (μm) | H_{ch} (μm) | L (cm) | N | T_{sat} ($^{\circ}\text{C}$) | x_{in} | x_{out} | G ($\text{kg/m}^2\cdot\text{s}$) |
|----------|-------------------------------|----------------------------|-------------------------------|-------------|-----|-------------------------------------|----------|-----------|-----------------------------------------|
| R134a | 200 | 100 | 600 | 1.0 | 25 | -26.37 | 0.1 | 1.0 | 348.8 |
| HFE 7100 | 200 | 100 | 600 | 1.0 | 25 | 59.63 | -1.0 | -0.1 | 663.2 |

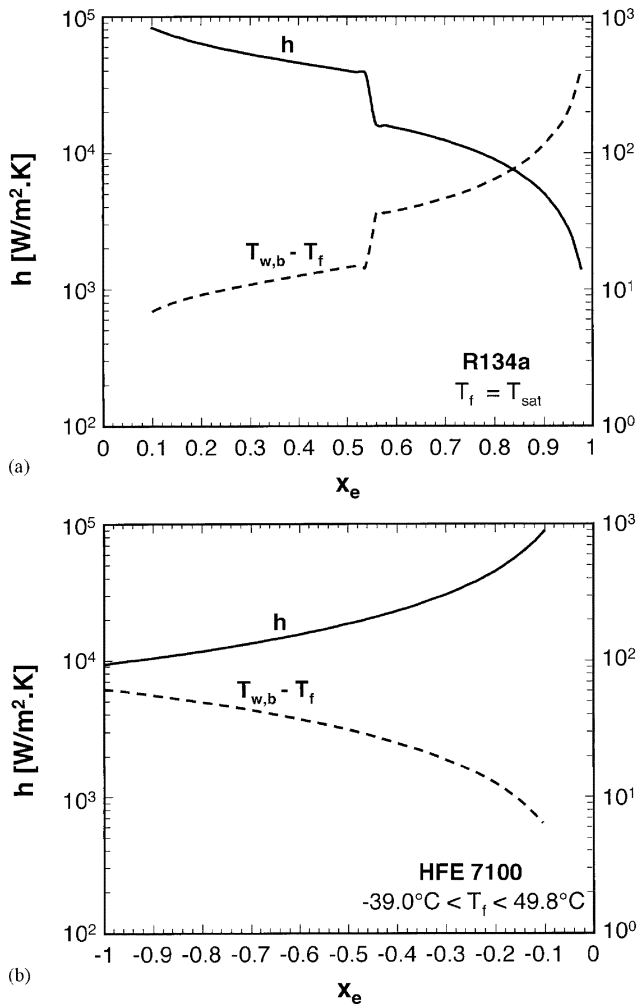


Fig. 9. Predictions of heat transfer coefficient versus thermodynamic equilibrium quality for (a) R134a saturated boiling in direct refrigeration cooling system and (b) HFE 7100 subcooled boiling in indirect refrigeration cooling system.

Fig. 9(b) shows the predictions for the HFE 7100 subcooled boiling case. Here, the heat transfer coefficient follows a trend opposite to that of R134a. The heat transfer coefficient increases and wall-to-fluid temperature difference decreases along the microchannel. Because the fluid temperature also increases along the microchannel, the wall temperature does not increase as it does with R134a, and may therefore be reduced by reducing the fluid inlet temperature. This is a key advantage of the indirect-refrigeration-cooling system.

Fig. 10 provides a summary of flow regimes and heat transfer regimes for microchannels, which is based on findings from both the saturated and subcooled boiling experiments and the above predictions. The existence of all the depicted regimes

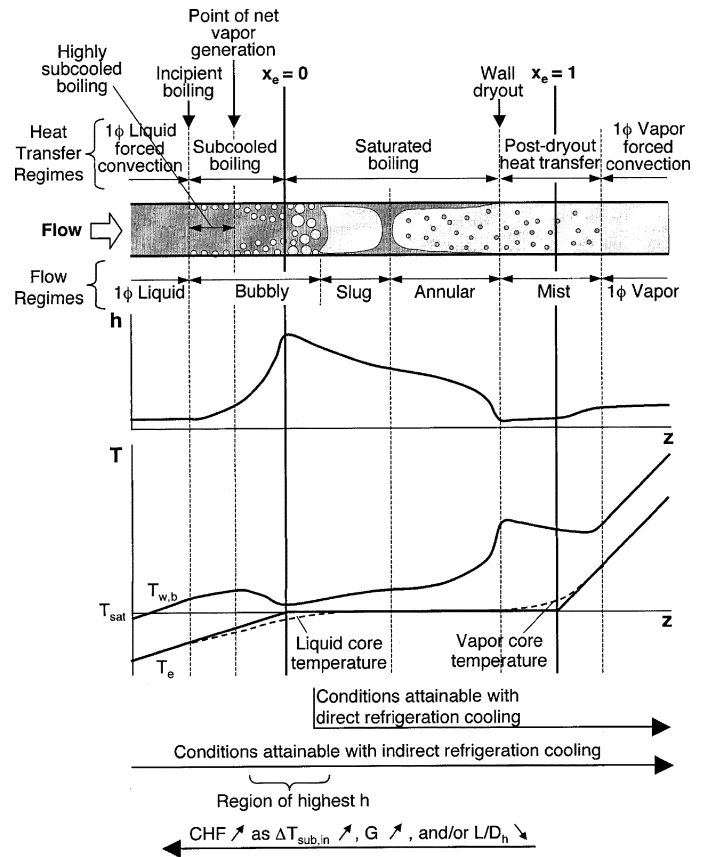


Fig. 10. Flow regimes, heat transfer regimes, and variations of wall temperature and convective heat transfer coefficient along microchannel flow.

assumes a fairly long heated channel. With a subcooled inlet, liquid flow persists for a finite length until boiling commences along the wall, marking the transition to subcooled boiling. Notice that the subcooled boiling region is comprised of two subregions. The upstream highly subcooled region precludes any appreciable bubble growth or entrainment of bubbles into the liquid core. As more of the wall liquid is heated above the saturation temperature, condensation along the bubble interface becomes weaker and bubbles are able to grow larger as well as depart into the liquid core. The transition point between the two subcooled subregions is termed the "point of net vapor generation." The saturated boiling region, which consists of bubbly, slug, and annular flow commences at the axial location where $x_e = 0$. This annular flow region persists until the point of wall dry-out. Droplets are still entrained in the vapor downstream from the dry-out point, providing post-dry-out mist flow. Eventually, all the droplets are consumed by evaporation and the flow is converted into pure vapor. Notice in Fig. 10 how the heat transfer coefficient is both constant and fairly low in

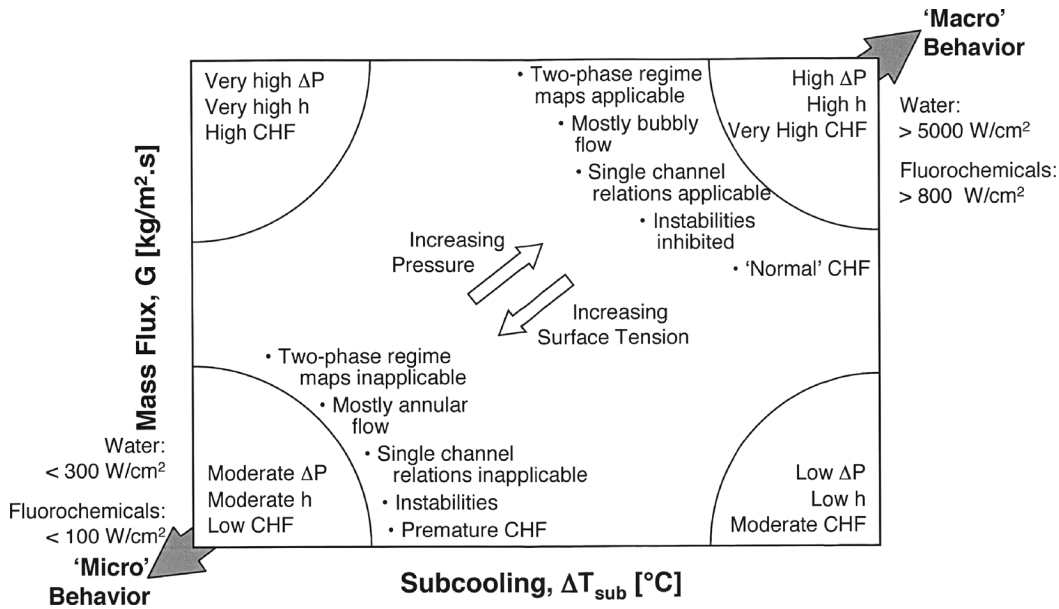


Fig. 11. Overall performance trends of small-diameter ($50 \mu\text{m} < d_h < 1000 \mu\text{m}$) two-phase microchannel heat sinks.

the inlet liquid region. The heat transfer coefficient begins increasing at the point of incipient boiling and reaches a maximum around $x_e = 0$. This is followed by a reduction in h in the saturated boiling region, reaching a minimum at the dry-out point. Fig. 10 also shows the variation of wall temperature along the microchannel. Lowest wall temperatures are encountered in the highly subcooled region and around $x_e = 0$.

Notice that, while the indirect-refrigeration-cooling system can attain all of the flow regimes and heat transfer regimes depicted in Fig. 10 (assuming the microchannel is long enough), the direct-refrigeration-cooling system can only sustain flow and heat transfer regimes corresponding to $x_e > 0$. However, the effectiveness of a microchannel cooling system depends not only on h , but the ability to avoid CHF. Fig. 7 shows higher CHF values are achieved with subcooled boiling. Subcooled boiling can generally be sustained by increasing inlet subcooling, increasing mass velocity, and/or decreasing the microchannel's length-to-diameter ratio.

From a system's point of view, the indirect refrigeration system offers the advantages of greater flexibility in controlling quality. In contrast, the compressor in a direct refrigeration loop requires maintaining a microchannel exit quality of 1.0 or greater. Another practical attribute of the indirect cooling system is the ability to operate the microchannel heat sink at a relatively mild pressure, compared to relatively high pressure for the direct cooling system, which is undesirable for electronic cooling because of structural concerns and added weight of the cooling module.

Fig. 11 shows, in a mass velocity—subcooling plane, the complex performance trends of a microchannel cooling system. Increasing mass velocity increases both the convective heat transfer coefficient and CHF. However, these advantages are realized at the expense of greater pressure drop. The convective heat transfer coefficient can also be increased by decreasing the inlet subcooling. Unfortunately, this also increases pressure drop and, more importantly, operation at low subcooling may

not be possible because of low CHF. Overall, the highest possible cooling heat fluxes (i.e., highest CHF) are achieved by increasing both mass velocity and subcooling.

Fig. 11 also sheds some light on one of the most illusive aspects of fluid flow and heat transfer in small diameter channels: the differences between microchannel and macrochannel behavior. Generally speaking, conditions that yield very high void fractions for a given diameter, namely low mass velocity and low subcooling, are more representative of "microchannel" behavior. Conversely, conditions that yield relatively low void fractions for a given diameter, namely, high mass velocity and high subcooling, resemble those of "macro-channel" flow. The former "microchannel" extreme is where conventional two-phase regime maps cease to apply, and where interaction between channels induces appreciable instability and premature CHF. The latter "macrochannel" extreme is where two-phase regimes are applicable, instabilities are inhibited, CHF is very high, and heat sink flow behavior follows that of single macrochannels. Notice how increasing pressure decreases the void fraction, pushing the entire system further towards the "macrochannel" extreme, while increasing surface tension produces larger bubbles and higher void fractions, pushing the system towards the "microchannel" extreme.

V. CONCLUSION

This study explored the use of low temperature refrigeration to maintain low device temperatures while dissipating high heat fluxes. Both direct- and indirect-refrigeration-cooling configurations were examined. In the direct cooling system, a microchannel heat sink serves as an evaporator in a conventional vapor compression cycle using R134a as working fluid. In the indirect cooling system, HFE 7100 is used to cool the heat sink in a liquid loop that rejects the heat to a secondary refrigeration loop. Key findings from the study are as follows.

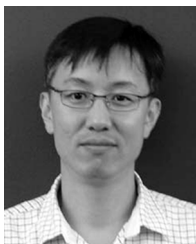
- 1) Two drastically different flow behaviors were observed in these systems. Because of compressor performance

constraints, mostly high void fraction two-phase flow patterns prevail in the R134a system, dominated by saturated boiling. On the other hand, the indirect-refrigeration-cooling system facilitates highly subcooled boiling inside the microchannel heat sink.

- 2) Different pressure drop trends were observed between the two systems. With R134a saturated boiling, pressure drop increases with increasing heat flux, but this increase becomes milder as most of the flow is converted to vapor. Pressure drop with HFE 7100 subcooled boiling first decreases with increasing heat flux because of decreasing viscosity in the single-phase liquid region. Pressure drop begins increasing following the commencement of boiling. Increasing mass velocity at high fluxes actually decreases pressure drop because of a reduction in void fraction.
- 3) The convective heat transfer coefficient for the R134a and HFE 7100 systems follow opposite trends relative to thermodynamic equilibrium quality. For R134a, the heat transfer coefficient is highest near $x_e = 0$ and decreases monotonically with increasing x_e . On the other hand, the convective heat transfer coefficient for HFE 7100 increases with increasing x_e below $x_e = 0$. Highest h values are about equal for the two fluids.
- 4) While the R134a system can produce fairly large h values, its cooling performance is limited by low CHF. Because of its high CHF, the indirect cooling system is far better suited for high-flux heat dissipation. Tests with this system yielded cooling heat fluxes as high as 840 W/cm^2 without encountering CHF.
- 5) The results from both systems provide a global understanding of the cooling behavior of microchannel heat sinks. These results are combined to construct a map of performance trends relative to mass velocity, subcooling, pressure, and surface tension. Extreme conditions of near-saturated flow, low mass velocity, low pressure and high surface tension point to "microchannel" behavior, where macrochannel flow pattern maps fail to apply, instabilities are prominent, and CHF is quite low. On the other hand, systems with high mass velocity, high subcooling, high pressure, and low surface tension are far more stable and yield very high CHF values; two-phase flow in these systems follows the fluid flow and heat transfer behavior, as well as the flow pattern maps of "macrochannels."

REFERENCES

- [1] I. Mudawar, "Assessment of high-heat-flux thermal management schemes," *IEEE Trans. Compon. Packag. Technol.*, vol. 24, no. 2, pp. 122–141, Jun. 2001.
- [2] R. K. Kirschman, "Cold electronics: An overview," *Cryogenics*, vol. 25, pp. 115–122, 1985.
- [3] P. E. Phelan, V. A. Chiriac, and T.-Y. T. Lee, "Current and future miniature refrigeration cooling technologies for high power microelectronics," *IEEE Trans. Compon. Packag. Technol.*, vol. 25, no. 3, pp. 356–365, Sep. 2002.
- [4] J. W. Peeples, W. Little, R. Shmidt, and M. Nisenoff, "Low temperature electronics workshop," in *Proc. 16th Semicond. Thermal Meas. Manag. Symp.*, San Jose, CA, 2000, pp. 108–109.
- [5] R. R. Schmidt and B. D. Notohardjono, "High-end server low-temperature cooling," *IBM J. Res. Develop.*, vol. 46, pp. 739–751, 2002.
- [6] V. Chiriac and F. Chiriac, "The optimization of a refrigerant vapor compression system for power microelectronics," in *Proc. ITHERM'06*, San Diego, CA, May–Jun. 30–6, 2006, pp. 759–764.
- [7] R. Wadell, Y. K. Joshi, and A. G. Fedorov, "Experimental investigation of compact evaporators for ultralow temperature refrigeration of microprocessors," *ASME J. Electron. Packag.*, vol. 129, pp. 291–299, 2007.
- [8] W. Qu and I. Mudawar, "Measurement and prediction of pressure drop in two-phase micro-channel heat sinks," *Int. J. Heat Mass Transfer*, vol. 46, pp. 2737–2753, 2003.
- [9] M. B. Bowers and I. Mudawar, "High flux boiling in low flow rate, low pressure drop mini-channel and micro-channel heat sinks," *Int. J. Heat Mass Transfer*, vol. 37, pp. 321–332, 1994.
- [10] M. B. Bowers and I. Mudawar, "Two-phase electronic cooling using mini-channel and micro-channel heat sinks: Part 1- Design criteria and heat diffusion constraints," *ASME J. Electron. Packag.*, vol. 116, pp. 290–297, 1994.
- [11] M. B. Bowers and I. Mudawar, "Two-phase electronic cooling using mini-channel and micro-channel heat sinks: Part 2- Flow rate and pressure drop constraints," *ASME J. Electron. Packag.*, vol. 116, pp. 298–305, 1994.
- [12] K. Mishima and T. Hibiki, "Some characteristics of air-water two-phase flow in small diameter vertical tubes," *Int. J. Multiphase Flow*, vol. 22, pp. 703–712, 1996.
- [13] K. A. Triplett, S. M. Ghiaasiaan, S. I. Abdel-Khalik, A. LeMouel, and B. N. McCord, "Gas-liquid two-phase flow in microchannels Part II: Void fraction and pressure drop," *Int. J. Multiphase Flow*, vol. 25, pp. 395–410, 1999.
- [14] T. N. Tran, M.-C. Chyu, M. W. Wambsganss, and D. M. France, "Two-phase pressure drop of refrigerants during flow boiling in small channels: An experimental investigation and correlation development," *Int. J. Multiphase Flow*, vol. 26, pp. 1739–1754, 2000.
- [15] H. J. Lee and S. Y. Lee, "Pressure drop correlations for two-phase flow within horizontal rectangular channels with small heights," *Int. J. Multiphase Flow*, vol. 27, pp. 783–796, 2001.
- [16] M. Zhang and R. L. Webb, "Correlation of two-phase friction for refrigerants in small-diameter tubes," *Exp. Thermal Fluid Sci.*, vol. 25, pp. 131–139, 2001.
- [17] A. Kawahara, P. M.-Y. Chung, and M. Kawaji, "Investigation of two-phase flow pattern, void fraction and pressure drop in a microchannel," *Int. J. Multiphase Flow*, vol. 28, pp. 1411–1435, 2002.
- [18] W. Qu and I. Mudawar, "Flow boiling heat transfer in two-phase micro-channel heat sinks – I. Experimental investigation and assessment of correlation methods," *Int. J. Heat Mass Transfer*, vol. 46, pp. 2755–2771, 2003.
- [19] W. Qu and I. Mudawar, "Flow boiling heat transfer in two-phase micro-channel heat sinks – II. Annular two-phase flow model," *Int. J. Heat Mass Transfer*, vol. 46, pp. 2773–2784, 2003.
- [20] J. Lee and I. Mudawar, "Two-phase flow in high-heat-flux micro-channel heat sink for refrigeration cooling applications: Part I – Pressure drop characteristics," *Int. J. Heat Mass Transfer*, vol. 48, pp. 928–940, 2005.
- [21] J. Lee and I. Mudawar, "Two-phase flow in high-heat-flux micro-channel heat sink for refrigeration cooling applications: Part II – Heat transfer characteristics," *Int. J. Heat Mass Transfer*, vol. 48, pp. 928–940, 2005.
- [22] I. Mudawar, M. A. El-Masri, C. S. Wu, and J. R. Ausman-Mudawar, "Boiling heat transfer and critical heat flux in high-speed rotating liquid films," *Int. J. Heat Mass Transfer*, vol. 28, pp. 795–806, 1985.
- [23] I. Mudawar and M. B. Bowers, "Ultra-high critical heat flux (CHF) for subcooled water flow boiling – I. CHF data and parametric effects for small diameter tubes," *Int. J. Heat Mass Transfer*, vol. 42, pp. 1405–1428, 1999.
- [24] J. Lee and I. Mudawar, "Fluid flow and heat transfer characteristics of low temperature two-phase micro-channel heat sinks – Part 1: Experimental methods and flow visualization results," *Int. J. Heat Mass Transfer*, vol. 51, pp. 4315–4326, 2008.
- [25] J. Lee and I. Mudawar, "Fluid flow and heat transfer characteristics of low temperature two-phase micro-channel heat sinks – Part 2: Subcooled boiling pressure drop and heat transfer," *Int. J. Heat Mass Transfer*, vol. 51, pp. 4327–4341, 2008.
- [26] F. P. Incropera and D. P. Dewitt, *Fundamentals of Heat and Mass Transfer*, 5th ed. New York: Wiley, 2002.
- [27] J. Lee and I. Mudawar, "Implementation of microchannel evaporator for high-heat-flux refrigeration cooling applications," *ASME J. Electron. Packag.*, vol. 128, pp. 30–37, 2006.



Jaeseon Lee received the M.S. and Ph.D. degrees, both in mechanical engineering, from Purdue University, West Lafayette, Indiana, in 2004 and 2008, respectively. His graduate research was focused on thermal management of high heat flux electronics and fundamentals physics of two-phase flow and heat transfer.

Currently, he is working at the United Technologies Research Center (UTRC), E. Hartford, CT, as a Senior Research Engineer/Scientist.



Issam Mudawar received the M.S. and Ph.D. degrees from the Massachusetts Institute of Technology, Cambridge, in 1980 and 1984, respectively. His graduate work involved magnetohydrodynamic (MHD) energy conversion and phase-change water cooling of turbine blades.

He joined the Purdue University School of Mechanical Engineering in 1984, where he established, and became Director of, the Boiling and Two-Phase Flow Laboratory (BTPFL) and Purdue University International Electronic Alliance (PUIECA). His work has been focused on phase change processes, thermal management of electronic and aerospace devices, intelligent materials processing, hydrogen storage, high-Mach turbine engines, and nuclear reactor safety. His theoretical and experimental research encompasses sensible and evaporative heating of thin films, pool boiling, flow boiling, jet-impingement cooling, spray cooling, microchannel heat sinks, heat transfer enhancement, heat transfer in rotating systems, critical heat flux, and capillary pumped flows. He is also President of Mudawar Thermal Systems, Inc., a firm that is dedicated to the development of thermal management solutions.

Prof. Mudawar received several awards for his research accomplishments, including the Best Paper Award in Electronic Cooling at the 1988 National Heat Transfer Conference, the Best Paper Award in Thermal Management at the 1992 ASME/JSME Joint Conference on Electronic Packaging, the *Journal of Electronic Packaging* Outstanding Paper of the Year Award for 1995, and the Best Paper Award in Thermal Management at ITherm 2008. He also received several awards for excellence in teaching and service to Purdue students and their organizations, including the Solberg Award for Best Teacher in School of Mechanical Engineering (1987, 1992, 1996, and 2004), the Charles Murphy Award for Best Teacher at Purdue University (1997), and the National Society of Black Engineers Professor of the Year Award (1985 and 1987). He was named Fellow of the American Society of Mechanical Engineers (ASME) in 1998.